Controlled Source Electromagnetic interferometry: the illumination function

Jürg Hunziker, Joost van der Neut, Evert Slob and Kees Wapenaar, Delft University of Technology, Yuanzhong Fan and Roel Snieder, Colorado School of Mines*

SUMMARY

With interferometry for controlled-source data, a reflection response can be retrieved as if the sources are relocated at receiver positions, which are for example in a borehole in seismics or at the ocean bottom in Controlled-Source Electromagnetics. Interferometry can be done with a cross-correlation process or with a multidimensional deconvolution process. We show that interferometry by cross-correlation, which assumes a lossless medium, is related to interferometry by multidimensional deconvolution via the illumination function. This illumination function can be used to judge the improvements of multidimensional deconvolution over cross-correlation interferometry, without actually computing the expensive matrix inversion in the multidimensional deconvolution approach.

INTRODUCTION

In geophysics, interferometry is mainly known from seismics as the process of cross-correlating two traces at two receiver positions to retrieve the Green's function between these two receivers (Schuster et al., 2004; Snieder, 2006). In a controlled-source experiment, interferometry is for example applied to redatum the sources to receiver positions in a borehole (Bakulin and Calvert, 2006; Vasconcelos et al., 2008; Minato et al., 2009). Since interferometry by cross-correlation (CC) assumes the medium to be lossless, CC is replaced by a multidimensional deconvolution (MDD) approach in lossy media (Wapenaar et al., 2008b; Schuster and Zhou, 2006). MDD consists mainly of two steps: First the data need to be decomposed into up- and downgoing wavefields and then, in a second step, the upgoing field is deconvolved with the downgoing field to retrieve the reflection response. The sources are thereby redatumed to the receiver locations, the direct field is eliminated and the medium above the receivers is replaced by a homogeneous half-space with the same material parameters as the surrounding of the receivers.

In electromagnetics, interferometry by MDD is mostly applied (Slob, 2009; Fan et al., 2009), because no lossless medium needs to be assumed. In this paper, we focus on marine Controlled-Source Electromagnetics (CSEM). We aim to remove the water-layer by interferometry, such that the disturbing effects related to the air-water interface (e.g. the airwave (Amundsen et al., 2006)) are eliminated. Note, that not only wavefields, but also diffusive electromagnetic fields can be decomposed (Amundsen et al., 2006; Slob, 2009; Wapenaar et al., 2008b). In that case we speak of downward- and upward-decaying fields. A comprehensive overview on all aspects of interferometry is given by Wapenaar et al. (2008a) and Schuster (2009).

Interferometry by CC and by MDD are related to each other through the illumination function (van der Neut and Thorbecke, 2009). We show that this illumination function can be used to diagnose how well the reflection response is retrieved by CC interferometry. In other words, the illumination function can be used to judge whether the amount of losses present in the data is small and interferometry by CC can be used for the retrieval of the reflection response or whether the losses are large and the more CPU-expensive MDD approach has to be chosen.

In this paper we first introduce the illumination function, which is then illustrated using an example from seismic interferometry and finally we focus on interferometry for marine Controlled-Source Electromagnetics with the aim to remove all effects of the air-water interface.

THEORY

The theory discussed here holds for seismic wavefields as well as for diffusive electromagnetic fields. The seismic wavefields can be decomposed into flux-normalized upgoing and downgoing wavefields using an algorithm derived by Wapenaar et al. (2008b) and the electromagnetic fields can be decomposed into flux-normalized up- and downward-decaying fields using an algorithm derived by Slob (2009). The decomposition can be done at any depth level where no sources are present. The implementation used here assumes the material parameters to be laterally constant at the depth level of decomposition. Note that in seismics the decomposition is sometimes approximated with time-gating. This can not be done in electromagnetics since there is no arrival time information and all events overlap. Upgoing or upward-decaying fields are represented by $\hat{\mathbf{P}}^-$ and downgoing or downward-decaying fields by $\hat{\mathbf{P}}^+$. The circumflex denotes space-frequency domain quantities. The quantities $\hat{\mathbf{P}}^-$ and $\hat{\mathbf{P}}^+$ are written in matrix notation, where each column contains various receiver positions for a fixed source position and vice versa for the rows (Berkhout, 1982). The decomposed fields are related to each other through the reflection response matrix $\hat{\mathbf{R}}_0^+$

$$\hat{\mathbf{P}}^- = \hat{\mathbf{R}}_0^+ \hat{\mathbf{P}}^+. \tag{1}$$

The matrix product on the right side is in this notation equivalent to an integration over all receivers. The reflection response $\hat{\mathbf{R}}_0^+$ is what we aim to retrieve using interferometry by MDD. The superscript $^+$ in the reflection response indicates that its origin is a downgoing or a downward-decaying field and the subscript $_0$ represents the absence of heterogeneities above the receiver level. Equation 1 can be solved for $\hat{\mathbf{R}}_0^+$ in a least-squares sense

$$\hat{\mathbf{R}}_0^+ = \hat{\mathbf{P}}^- \left(\hat{\mathbf{P}}^+\right)^\dagger \left[\hat{\mathbf{P}}^+ \left(\hat{\mathbf{P}}^+\right)^\dagger + \varepsilon^2 \mathbf{I}\right]^{-1}, \tag{2}$$

where the superscript † denotes complex-conjugation and transposition. The stabilization parameter ε stabilizes the inversion

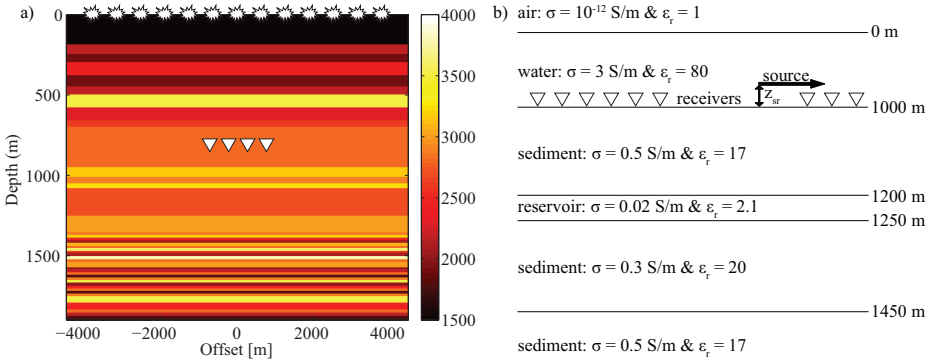

Figure 1: Setup of the numerical modeling: a) Seismic model: P-wave velocities in m/s. White triangles indicate the location of the receivers in a horizontal borehole, white explosion symbols are located at the source positions. b) Electromagnetic model: The black arrow indicates the source, white triangles the receivers. Conductivity σ and relative permittivity ε_r are given for each layer. The vertical source-receiver distance z_{sr} is chosen 25 m for the first case and 825 m for the second case.

and $\mathbf{I}$ is the identity matrix. Equation 2 can be rewritten as follows

$$\hat{\mathbf{D}} = \hat{\mathbf{C}} \left[\hat{\Gamma} + \varepsilon^2 \mathbf{I} \right]^{-1}, \tag{3}$$

where

$$\hat{\mathbf{D}} = \hat{\mathbf{R}}_{\mathbf{0}}^{+}, \tag{4}$$

$$\hat{\mathbf{C}} = \hat{\mathbf{P}}^{-} \left(\hat{\mathbf{P}}^{+} \right)^{\dagger} \quad \text{and} \tag{5}$$

$$\hat{\Gamma} = \hat{\mathbf{P}}^{+} \left(\hat{\mathbf{P}}^{+} \right)^{\dagger}. \tag{6}$$

In this way, the reflection response $\hat{\mathbf{R}}_0^+$ can be seen as the result of a deconvolution process $\hat{\mathbf{D}}$, where the cross-correlation $\hat{\mathbf{C}}$ of $\hat{\mathbf{P}}^+$ with $\hat{\mathbf{P}}^-$ is deconvolved with the illumination function $\hat{\Gamma}$. In seismics it has been shown, that if the illumination function $\hat{\Gamma}$ is close to a spike, the cross-correlation $\hat{\mathbf{C}}$ can be a good approximation for the reflection response and the CPU-expensive deconvolution becomes unnecessary. Thus, the illumination function $\hat{\Gamma}$ can be used to investigate the improvements of the deconvolution process with respect to the cross-correlation without computing the deconvolution (van der Neut and Thorbecke, 2009). In electromagnetics, the illumination function can be used in the same way as in seismics, what will be shown in this paper.

RESULTS: SEISMICS

First we have a look at the illumination function $\hat{\Gamma}$ in seismics, where it was originally derived. We illustrate its significance with a synthetic example featuring a layered Earth structure including a free surface. We modeled seismic data in an elastic dissipative medium with a finite difference code of Robertsson et al. (1994), with overall loss terms for P-waves $Q_P = 21$ and S-waves $Q_S = 16$ incorporated. P-wave velocities are shown in Figure 1a. The 501 2-component (vertical and horizontal force) sources are located just below the earth's surface with 16 m spacing and the 101 4-component receivers are located in a horizontal well at 800 m depth with 16 m spacing as well.

Our aim is to redatum the sources to the receiver array by seismic interferometry. For this purpose we decompose the data at the receiver level in up- and downgoing P- and S-wave constituents, making up the matrices $\hat{\mathbf{P}}^-$ and $\hat{\mathbf{P}}^+$ as discussed in the theory section. The up- and downgoing wavefields are cross-correlated (equation 5), yielding the cross-correlation matrix $\hat{\mathbf{C}}$. This matrix can be computed at each frequency, yielding a cross-correlation cube. We evaluated a slice of this cube for a retrieved source at the central receiver location, see Figure 2a. If the overburden were lossless and homogeneous and if the free surface were absent, this slice could be interpreted as the reflection response in the space-frequency domain of a virtual P-wave source at the central receiver location and P-wave receivers at the other receiver locations (Mehta et al., 2007; Wapenaar et al., 2008b). For comparison, we computed a directly modeled reflection response in the space-frequency domain by placing an active source at the central receiver location, see Figure 2b. Note that Figures 2a and b are not identical, or $\hat{\mathbf{C}} \neq \hat{\mathbf{R}}_0^+$, which can mainly be contributed to the attenuation in the medium. The mismatch can be diagnosed directly by study of the illumination function $\hat{\Gamma}$. We computed the illumination function for a virtual source at the central receiver location, see Figure 2c. The cross-correlation function $\hat{\mathbf{C}}$ (Figure 2a) can be interpreted as the desired reflection response $\hat{\mathbf{R}}_0^+$ (Figure 2b) blurred spatially and temporally with $\hat{\Gamma}$ (Figure 2c). If the assumptions for interferometry by CC are well fulfilled, the illumination function will resemble a bandlimited spike in the space-time domain, leading to a flat spectrum in the frequency direction and a bandlimited delta function in the space direction in the space-frequency domain. If the illumination function does not exhibit this behavior, such as in Figure 2c, the redatumed source will carry the imprint of this function. Since $\hat{\Gamma}$ can be estimated from the data, $\hat{\mathbf{C}}$ can be deblurred by implementation of equation 3, which gives the deconvolution function $\hat{\mathbf{D}}$. This process is referred to as MDD. The space-frequency representation of the retrieved reflection response after MDD is shown in Figure 2d. Note indeed that $\hat{\mathbf{D}}$ (Figure 2d) has converged closer to the desired reflection response $\hat{\mathbf{R}}_0^+$ (Figure 2b). This convergence could also be observed in other domains and for other components.

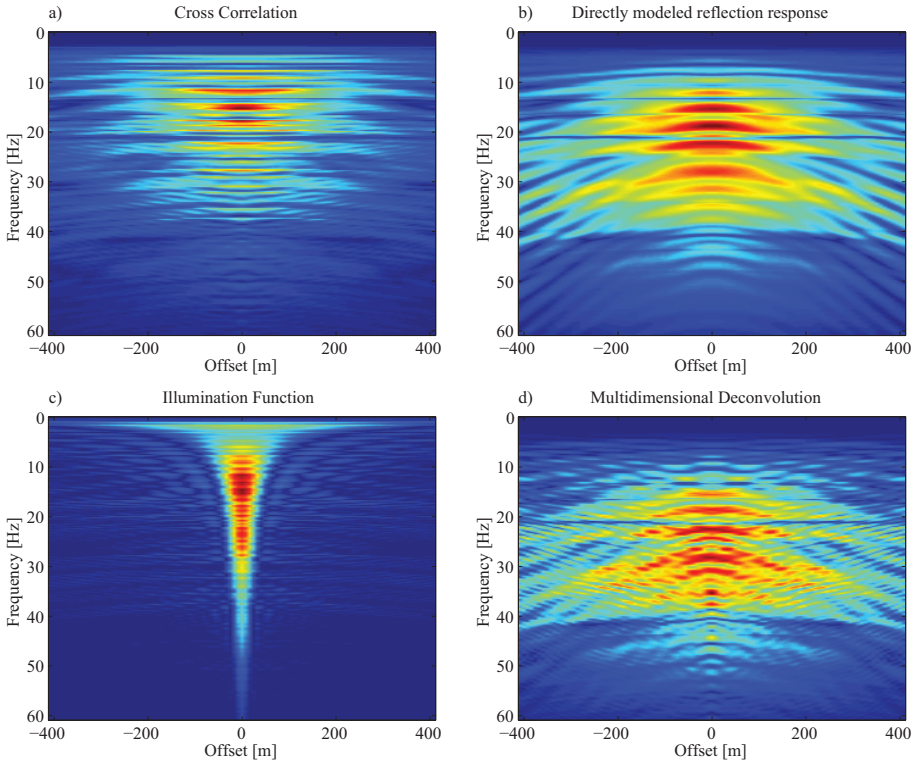

Figure 2: P-P Reflection responses and illumination function in seismics in the space-frequency domain. Subfigure a) shows the reflection response retrieved by cross-correlation $\hat{\mathbf{C}}$, b) the directly modeled reflection response $\hat{\mathbf{R}}_0^+$, c) the illumination function $\hat{\Gamma}$ and d) the reflection response retrieved by MDD $\hat{\mathbf{D}}$. The blue color represents low and the red color large amplitudes.

RESULTS: ELECTROMAGNETICS

The steps applied to the seismic dataset can be implemented in the same way to diffusive electromagnetics as CSEM, with the goal to remove all effects related to the water-layer. Two synthetic 2D Transverse Magnetic CSEM-datasets in a configuration that consists from top to bottom of a half-space of air, a water layer and half-space of several sedimentary layers are modeled. The sedimentary halfspace is intersected by a reservoir layer. The electric source is oriented parallel to the line of receivers generating a monochromatic signal at a frequency of 0.5 Hz. The resulting Earth response is recorded by inline electric E_x and crossline magnetic H_y receivers at the sea floor. The difference between the two datasets is the position of the source within the water layer. In the first case the source is located 25 m above the receivers, to simulate a typical CSEM measurement with the source close to the receivers, henceforth referred to as traditional case. In the second case, the source is positioned 825 m above the receivers, representing an experiment with the source at shallower depth, henceforth referred as experimental case. In both cases the water layer has a thickness of 1000 m. All the electrical and geometrical parameters are given in Figure 1b.

The reflection response retrieved by cross-correlation $\hat{\mathbf{C}}$ is normalized and plotted in Figures 3a and b for the traditional and the experimental case, respectively. It is compared with a directly modeled reflection response, which is normalized as well. The directly modeled reflection response is the correct solution which was found by modeling. Figure 3 is for a single frequency, hence functions depend on distance only, whereas in Figure 2 the functions depend on frequency and offset. It can be seen, that in the traditional case, $\hat{\mathbf{C}}$ is relatively close to the directly modeled reflection response except around an offset of 1000 m where the side lobes of the reflection response are retrieved incorrectly, but one should be aware that this is only the case after normalization, since the amplitudes are not correctly retrieved at all. In the experimental case, the shape of the reflection response retrieved by cross-correlation does not match that well with the directly modeled reflection response. Instead, $\hat{\mathbf{C}}$ is broadened in Figure 3b with respect to the directly modeled reflection response. As in seismics this is due to the attenuation and the free surface which interferometry by CC does not take into account. Since the energy has to diffuse for a longer distance through the water in the experimental case, $\hat{\mathbf{C}}$ is more severely affected by the attenuation than is the case in the traditional situation, which leads to the described broadening of $\hat{\mathbf{C}}$.

To retrieve $\hat{\mathbf{D}}$, $\hat{\mathbf{C}}$ is deconvolved with the illumination function $\hat{\Gamma}$ (equation 3), which is shown in Figures 3c and d for the traditional and the experimental case, respectively. Since the shape of the reflection response was already retrieved quite well in the traditional case, deconvolution with $\hat{\Gamma}$ mainly corrects for the amplitude (Figure 3c). Therefore, the illumina-

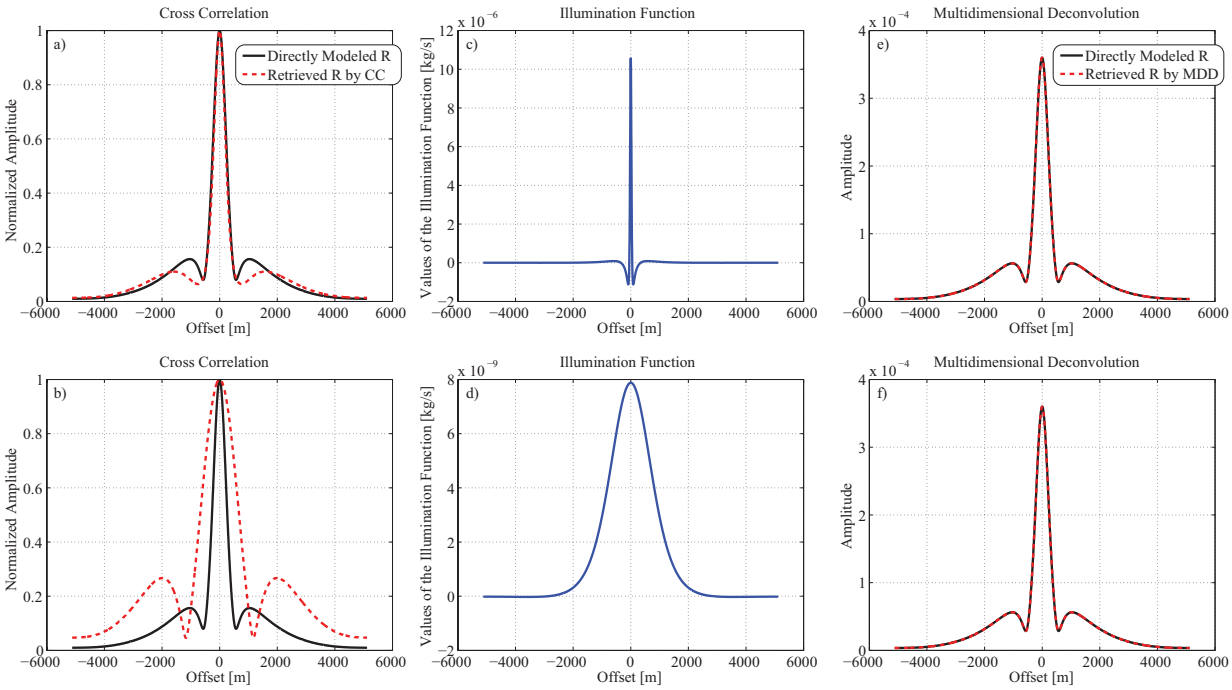

Figure 3: The reflection response (R) retrieved by cross-correlation $\hat{\mathbf{C}}$ is shown in subfigures a) and b) for the traditional and the experimental case, respectively. Note that the amplitudes have been normalized. Subfigures c) and d) show the illumination function $\hat{\Gamma}$ with blue curves for the traditional and the experimental case, respectively, and subfigures e) and f) show the reflection response retrieved by MDD $\hat{\mathbf{D}}$ for the traditional and the experimental case, respectively. The reflection responses (red curves) are compared with the directly modeled reflection responses (black).

tion function is almost a spike. In the experimental case, the deconvolution with $\hat{\Gamma}$ has also to correct for the broadening of the reflection response. Consequently, $\hat{\Gamma}$ is much broader. In other words, the illumination function contains information about how well the reflection response has been retrieved by cross-correlation.

Finally, the reflection response retrieved by MDD is shown in Figures 3e and f for the two cases. The comparison with the modeled reflection response shows, that MDD retrieved the reflection response perfectly. Furthermore, the two reflection responses are the same for both source geometries. Consequently, the deconvolution of $\hat{\mathbf{C}}$ with $\hat{\Gamma}$ has compensated perfectly for the attenuation. Also the dependence of all effects related to the water-layer, including the position of the source, have been removed successfully.

In CSEM the data are often quantitatively compared to a reference dataset which was acquired over a region without a reservoir in the subsurface. The difference is normally rather small and visible only at intermediate offsets, because at short offsets the fields are dominated by the direct field and at large offsets by the airwave (Amundsen et al., 2006). Since all effects related to the water layer are removed with interferometry, the resulting reflection response exhibits a larger difference from the reflection response of the reference dataset than the original data do and the difference is significant at all offsets. For such a comparison, the retrieval of correct amplitudes is crucial, which are only retrieved by MDD and not by CC.

CONCLUSIONS

We have demonstrated for seismics and electromagnetics, that the illumination function can be used to judge the improvements of interferometry by multidimensional deconvolution with respect to interferometry by cross-correlation without computing the CPU-expensive deconvolution step. Furthermore, we have shown that in Controlled Source Electromagnetics with increasing source-receiver distance, for which the energy has to diffuse through the water, the illumination function becomes broader. Assuming dense enough sampling to decompose the fields properly, the deconvolution corrects perfectly for all the attenuation such that it is no longer relevant where the original electric source in the water was located. Additionally, in our examples, multidimensional deconvolution retrieved correct amplitudes, whereas cross-correlation was in the best case only capable of retrieving an almost correct shape, but incorrect amplitudes.

ACKNOWLEDGMENTS

This research is supported by the Dutch Technology Foundation STW, applied science division of NWO and the Technology Program of the Ministry of Economic Affairs (grant DCB.7913).

REFERENCES

Amundsen, L., L. Løseth, R. Mittet, S. Ellingsrud, and B. Ursin, 2006, Decomposition of electromagnetic fields into upgoing and downgoing components: Geophysics, **71**, G211–G223.

Bakulin, A. and R. Calvert, 2006, The virtual source method: Theory and case study: Geophysics, **71**, SI139–SI150.

Berkhout, A. J., 1982, Seismic migration. imaging of acoustic energy by wave field extrapolation: Elsevier.

Fan, Y., R. Snieder, and J. Singer, 2009, 3-d controlled source electromagnetic (CSEM) interferometry by multi-dimensional deconvolution: 79th Annual International Meeting, SEG, Expanded Abstracts.

Mehta, K., A. Bakulin, J. Sheiman, R. Calvert, and R. Snieder, 2007, Improving the virtual source method by wavefield separation: Geophysics, **72**, V79–V86.

Minato, S., T. Matsuoka, T. Tsuji, D. Draganov, J. Hunziker, and K. Wapenaar, 2009, Application of seismic interferometry by multidimensional deconvolution to crosswell seismic reflection using singular-value decomposition: 79th Annual International Meeting, SEG, Expanded Abstracts.

Robertsson, J. O. A., J. O. Blanch, and W. W. Symes, 1994, Viscoelastic finite-difference modeling: Geophysics, **59**, 1444.

Schuster, G., 2009, Seismic interferometry: Cambridge University Press.

Schuster, G. and M. Zhou, 2006, A theoretical overview of model-based and correlation-based redatuming methods: Geophysics, **71**, SI103–SI110.

Schuster, G. T., J. Yu, J. Sheng, and J. Rickett, 2004, Interferometric/daylight seismic imaging: Geophysical Journal International, **157**, 838–852.

Slob, E., 2009, Interferometry by deconvolution of multicomponent multioffset GPR data: IEEE Transactions on Geoscience and Remote Sensing, **47**, 828–838.

Snieder, R., 2006, Extracting the Green's function of attenuating heterogeneous acoustic media from uncorrelated waves: Journal of the Acoustical Society of America, **121**, 2637–2643.

van der Neut, J. and J. Thorbecke, 2009, Resolution function for controlled-source seismic interferometry: a data-driven diagnosis: 79th Annual International Meeting, SEG, Expanded Abstracts.

Vasconcelos, I., R. Snieder, and B. Hornby, 2008, Imaging internal multiples from subsalt VSP data - examples of target-oriented interferometry: Geophysics, **73**, S157–S168.

Wapenaar, K., D. Draganov, and J. O. A. Robertsson, 2008a, Seismic interferometry: history and present status: Society of Exploration Geophysicists.

Wapenaar, K., E. Slob, and R. Snieder, 2008b, Seismic and electromagnetic controlled-source interferometry in dissipative media: Geophysical Prospecting, **56**, 419–434.